Article:
Song, D. orcid.org/0000-0001-6360-3296, Wang, S. orcid.org/0000-0003-1609-5326, Zhang, Z. orcid.org/0000-0003-0204-3867 et al. (2 more authors) (2023) A Novel Continuum Overtube with Improved Triangulation for Flexible Robotic Endoscopy. IEEE Transactions on Medical Robotics and Bionics. ISSN 2576-3202

https://doi.org/10.1109/tmrb.2023.3294527

A Novel Continuum Overtube with Improved Triangulation for Flexible Robotic Endoscopy

Dezhi Song, Shuxin Wang, Zhiqiang Zhang, Xiangyang Yu, Chaoyang Shi

***Abstract*—This paper presents a novel continuum overtube that consists of a notched tendon-driven 2-DOF continuum joint and a distal deployable structure driven by a flexible screw rod. A smooth bending shape with constant curvature is achieved by adopting an overlapped area between notches to generate uniform stress distribution. The distal deployable structure provides an extensive triangulation for bimanual operations. The presented design achieves high flexibility, sufficient loading and anti-twisting capacity, and an improved layout of functional channels for flexible robotic endoscopy. Design optimization is performed to optimize structural parameters for performance investigation and improvement. The proposed continuum joint achieves an average distal positioning error of 1.48% and 1.20% within [-115°, 115°] in the two bending planes with minor hysteresis errors of less than 1.5%, indicating the outstanding constant bending curvature characteristics for kinematic modeling and control. The loading capacity achieves 4.27N and provides significant advantages in terms of sufficient rigidity over the commercial endoscope. The designed deployable structure has significantly improved operational triangulation, which can effectively support bimanual operations with two instruments for complex operations. Meanwhile, the torsional stiffness of the designed continuum joint reaches a considerable value of 8.73mNm/° and provides stable support for instruments during operations. Ex-vivo experiments of gastric tissue biopsy have been performed to verify the feasibility of the presented design in a practical scenario.**

***Index Terms*—Flexible endoscopy (FE), natural orifice transluminal endoscopic surgery (NOTES), continuum robot, minimally invasive surgery (MIS), design optimization**

I. Introduction

Flexible access surgery has demanded the development trend from rigid and straight surgical instruments in MIS to be shifted to flexible and continuum surgical manipulators [1, 2]. The robot-assisted natural orifice transluminal endoscopic surgery and flexible endoscopy are two emerging procedures for flexible access surgery. They typically utilize flexible endoscopes and instruments to wind through tortuous human intraluminal and transluminal paths from natural orifices for dexterous screening and treatment [3, 4]. As so-called no-incision or no-visible-scar procedures, they target tumor and cancer diagnosis and treatment in the early stage to achieve a significantly better prognosis and improved 5-year rates of survival [5], and meanwhile provide benefits in terms of minimized intraoperative trauma, reduced wound healing time, fewer pains, and lower risks of infection [6, 7]. The flexible robotic endoscopy typically involves applying a distal continuum-style overtube with excellent flexibility to guide the flexible endoscopic manipulator into the body and approach the lesion for further diagnostic examination and therapeutic options [8, 9], as shown in Fig. 1. Hence, the distal overtube is also required to possess high rigidity to produce sufficient interaction forces and maintain its shape stable for instruments during surgical operations. Besides, it is difficult for surgical instruments to be deployed in the confined digestive tract to complete the bimanual operation restricted by the physiological cavity size. Therefore, a deployable structure is also indispensable at the distal end of the continuum joint to provide a more extensive operational triangulation for two surgical instruments [10], as shown in Fig. 1. However, achieving flexible access and high loading capacity to address practical surgical scenarios for both diagnostic purposes and therapeutic procedures remains challenging [11, 12]. Therefore, the development of continuum joints that provide high flexibility and loading capacity and empower extensive triangulation has been emerging and attracting broad attention to target designing distal flexible overtubes for surgical endoscopic robots.

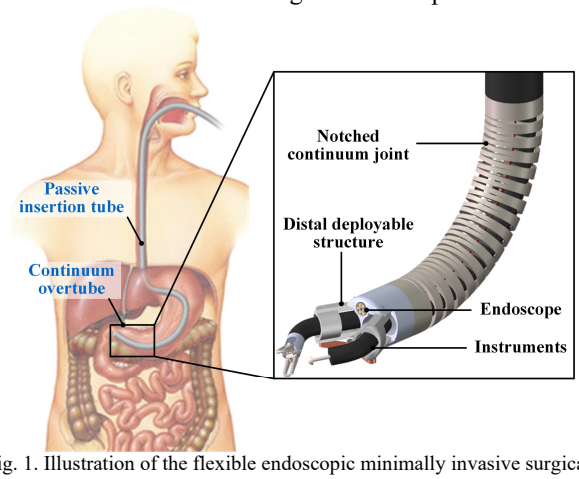

Fig. 1. Illustration of the flexible endoscopic minimally invasive surgical robots with two operational instruments.

Many attempts have been made to focus on designing the continuum joint for surgical applications [13]. The design scheme of the continuum joint can be generally grouped into two categories of discrete and continuum types. The first type

Mannuscript received Apr 14, 2023. This work is supported in part by National Natural Science Foundation of China under Grant 92148201, Grant 61973231, Grant 51721003, Grant 62211530111, and Royal Society under IEC\NSFC\211360. Corresponding author: C. Shi (chaoyang.shi@tju.edu.cn).

D. Song, S. Wang, C. Shi are with the Key Laboratory of Mechanism Theory and Equipment Design of Ministry of Education, School of Mechanical Engineering, Tianjin University, Tianjin 300072, China. Z. Zhang is with the School of Electronic and Electrical Engineering, University of Leeds, Leeds, LS2 9JT, UK. X. Yu is with the Department of Gastrointestinal Surgery, Tianjin Hospital of ITCWM/Tianjin Nankai Hospital, Tianjin, 300100, China.

of continuum joint is composed of a series of discrete rigid joints [14], such as hinged-based joints [15], revolved sliding joints [16], and rolling friction-based joints [17, 18], in which the bending motion relies on the kinematic pairs between joints. Zhang et al. [19] designed a constrained tendon-driven continuum mechanism (CTCM) based on spherical joints with 2-DOF and integrated it at the distal end of the UR5 robot for laparoscopic bariatric surgery and produced a bending angle of up to 60°. However, the spherical joint manufactured by 3D printing resulted in uneven contact between serpentines, which generated high friction nonlinearity and degraded the constant curvature property and the loading capability. Hong et al. [16-20] extended this design and increased the loading capacity for maxillary sinus surgery by embedding two Nitinol tubes inside to reduce one bending DOF. This improved design could achieve a bend angle of up to 270°, empower flexible access, and bear loading of 150g. However, when the bending deflection occurs at a large angle, the existing high friction between joints increases significantly, resulting in nonconstant curvature for the bending motion. To reduce the friction between the discrete joints, Kwang et al. [17] proposed a constrained continuum (CC) manipulator based on gear and auxiliary links with only 1-DOF suited for flexible endoscopic surgery. The prototype was designed within the bending range of ±90° and achieved a payload of 300g. However, the complex structural design and complicated assembly process led to challenges for both fabrication and integration, as well as rising production costs. In conclusion, the discrete-style continuum joint commonly suffers from high and uneven friction in a large deflection, leading to nonuniform bending curvature or inconsecutive shape. For the initial state, this category of the continuum joint tends to shrink into a zigzag shape due to static instability [21]. In addition, such joints typically face insufficient loading capacity without limiting DOF. Moreover, it is prone to cause perforation during access through the narrow and variable anatomical path due to its rigid and discrete structure [22-24]. Therefore, they are mainly applied for instrument design in flexible endoscopic surgery which does not require high accuracy of kinematic modeling.

The second category of the continuum joint is commonly designed based on a notched skeleton or helical spring-like structure and utilizes the material's elastic deformation to produce bending motions and generate a relatively smooth body shape. Gafford et al. [25] and Yash Chitalia et al. [26, 27] presented a notched continuum joint based on unidirectional asymmetric and bidirectional interlaced notches for otology and neurosurgery examination, respectively, and generated a bending range of [0, 90°]. However, each designed segment only possessed 1-DOF, and its deflection motion was accompanied by apparent axial compression, resulting in increased modeling error. Moreover, the loading capacity of this design was not experimentally validated or discussed. Lee et al. [28] designed a 2-DOF modularized continuum overtube by adopting the rectangular slit structure with rigid supporters to resist axis compression for NOTES. This design can deflect with a maximum angle of 90° and withstand an external loading of 7N. However, the complex structure resulted in a larger diameter of 23mm, and the design posed difficulties for bimanual operation due to a lack of consideration of triangulation. Besides, these rectangular notches are commonly arranged in an orthogonal sequence to achieve 2-DOF bending motion. The typical rectangular notch can only provide limited deformation for bending without fracture due to the small opening angle of the notch shape and the restricted overlapping area between notches. This design methodology makes it challenging to achieve a large bending angle and workspace without increasing the total length of the continuum joint [29, 30]. The triangular notched-based continuum joints have some advantages in bending performances compared with the rectangular-based ones. However, only 1-DOF deflection (bending in the 2D plane) can be achieved due to the lack of a specialized design for the structural parameters of notches [31, 32]. To achieve 2-DOF bending motion, the two-segment configuration is commonly utilized. However, it not only reduces dexterity due to the increased length of the bending section and curvature radius but also poses challenges for driving unit design and motion control of the continuum joint due to the coupling between different segments. The continuum joints based on helical structures were also implemented for flexible endoscopic surgery [33-37]. Song et al. [35] developed a 1-DOF flexible joint based on a helical structure to achieve an extensive bending range and adopted a rigid-flexible coupling design to enhance the loading capacity and achieved 5N when bent at 120°. However, the torsion resistance of the helical structure was limited, leading to unstable support for the instruments in flexible endoscopic surgery. The continuum-style joints commonly use materials' elastic properties to produce bending motion, thus generating large tension forces of driving tendons and supporting excellent loading capacity. However, they suffer from undesired axial compression during bending motion, increasing kinematic modeling errors. Besides, the anti-torsion capability for the design of continuum joints is also challenging, especially for the lengthy continuum structure. However, few attempts have been implemented and investigated. When the anti-torsion capacity is insufficient, the rotation consistency of the proximal and distal parts of the continuum joint can be noticeable, deteriorating the control accuracy. Moreover, the above-mentioned designs typically reserve a single working channel for one instrument, which can only complete diagnosis or simple therapeutic procedures. Thus, the existing implements lack consideration for bimanual operations such as endoscopic submucosal dissection (ESD) and endoscopic mucosal resection (EMR), in which the continuum overtube is required to provide a broad triangulation and maintain the visualization of the surgery area.

To cope with these drawbacks, this paper presents a novel continuum overtube consisting of a notched-based continuum joint with a central backbone and a distal deployable structure. The notched continuum structure has been designed and prototyped based on an array of deeply cut triangular notches. The distal deployable structure based on a four-bar mechanism has been proposed and integrated at the distal end of the joint

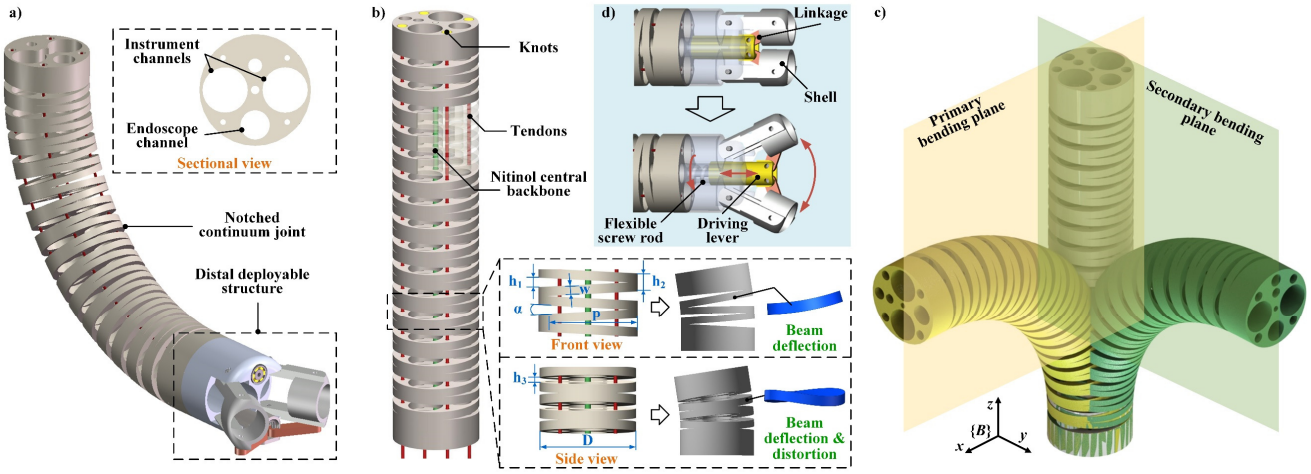

Fig.2. a) Design elucidation of the continuum overtube; b) The detailed structural design of the proposed continuum joint; c) The definition of the two bending planes; d) The proposed distal deployable structure.

and is driven by a flexible screw rod. The proposed continuum overtube offers advantages in terms of high flexibility, constant curvature characteristics for bending motions, sufficient loading and anti-twisting capability, improved layout of functional channels for surgical tools, and extensive operational triangulation. Design optimization is utilized to investigate and determine the structural parameters of the continuum overtube. Simulation and analysis have been performed to evaluate the influences of the designed deployable structure on the operational workspace and triangulation. The performance evaluation and ex-vivo bimanual biopsy experiments are implemented with the presented overtube design to investigate and validate its performances and effectiveness.

II. Materials and Methods

A. Design Specifications of the Proposed Continuum Overtube

This work targets designing a continuum overtube with improved triangulation for flexible endoscopy. The related design requirements have been summarized as follows: 1) The distal continuum joint commonly has two DOFs of deflection, and its bending range typically achieves more than 90° to perform the dexterous examination and accommodate internal instruments for surgical operations [28]. 2) The current designs of continuum joints/overtubes for robot-assisted flexible endoscopy typically range from 80mm to 120mm in length [28, 38]. 3) The distal continuum joints for flexible endoscopy are commonly embedded with three or four internal functional channels. If they are designed to carry two instrument channels for bimanual operation, their outside diameter values ranging from 16mm to 22mm are acceptable [39]. 4) Previous research has suggested that the estimated mean loading capacity required to manipulate mucosal tissue in the GI tract is smaller than 1.24N and will not exceed an upper limit of 2.26N [40].

B. Structural Design of the Proposed Continuum Overtube

1) Design of the distal continuum joint

The designed continuum overtube mainly consists of two parts that include a notched 2-DOF continuum joint and a distal deployable structure, as illustrated in Fig. 2a). The continuum joint utilizes the tendon-driven approach and adopts the triangular notched structure with a central Nitinol backbone to achieve 2-DOF bending motion, as illustrated in Fig. 2b). A 16mm outer diameter and an 80mm overall length are specified for this joint. The proposed notched-based continuum structure consists of an array of deeply cut and interlaced triangular notches along the axial direction. By adjusting the depth of these triangular notches to 14.5mm, the shape of the designed continuous notches can be considered a bidirectional asymmetric form from the front view; while its shape is approximately regarded to be a bidirectional symmetric form in the side view. The presence of a notched gap in both views makes it possible for the continuum joint to bend in two planes. However, the region that undergoes deformation during the bending process is exactly the area of overlap between the notches. This overlapping area can be regarded as a deformable beam [32]. It undergoes deflection when the continuum joint bends in the primary plane (XZ plane), and experiences both deflection and distortion when the continuum joint bends in the secondary plane (YZ plane), as shown in the lower right corner of Fig. 2b). Thus, the proposed continuum joint can achieve 2-DOF bending motion, as shown in Fig. 2c). The notched structure exhibits excellent property performances for improved workspace and high flexibility with constant bending curvature characteristics. The proposed deeply-cutting method of the triangular notches overcomes the limitation of a single DOF existing in most bidirectional asymmetric notched joints [27, 41, 42]. For a single-segment continuum joint, it significantly improves flexibility and the reachable workspace without additional driving elements. Besides, the specialized cutting increases the overlapping area between the notches, which distributes the stress more evenly when bent. Thus, the smooth bending shape of the designed joint can be obtained with constant curvature. A Nitinol rod (OD = 1.2mm) is utilized as the central backbone and fixed to both ends of the continuum joint to further prevent the irresistible axial compression of the continuum joint during bending so that the constant bending curvature assumption can be applied for kinematic modeling and control. The applied Nitinol rod passes through the central

hole of the continuum joint so that it is constrained by multiple points, which also helps prevent the buckling of the Nitinol rod due to its high slenderness ratio. The super-elastic characteristic of the central Nitinol rod further enhances the continuum joint's loading capacity. Besides, the combination of the notched structure and central backbone empowers the improved twisting resistance due to its integrated structure, providing stable support for surgical operations. Four pulling tendons pass through the holes arranged in the circumferential uniform distribution of the continuum joint and are fixed at the distal end by knots. Several functional channels are reserved within the joint to facilitate the integration with an endoscope and surgical instruments. The detailed nomenclature used in this work is listed in Table I.

TABLE I
NOMENCLATURE USED IN THIS WORK

Symbol	Description
h_1	Width of triangular notch in front view [mm]
h_2	Top width of triangular notch [mm]
h_3	Width of triangular notch in side view [mm]
p	Depth of triangular notch [mm]
w	Thickness of overlapping area between notches [mm]
α	Angle of triangular notch opening [deg]
θ	Angular deflection of the continuum overtube [deg]
n	The number of unilateral notches

2) Design of the distal deployable structure

The detailed design of the deployable structure has been illustrated in Fig. 2d). It primarily comprises two groups of symmetrically arranged four-bar mechanisms, and they share the same driving lever labeled in yellow. Pushing and pulling this lever can activate the outside shell for opening and closing operations. The reciprocating motion of the lever is driven by a specialized flexible screw rod that is retrofitted by a flexible shaft (MAISO, CN, OD = 1.5mm). The flexible screw rod can transfer torque with a torsional stiffness of approximately 0.135mNm/° inside both straight and curved pipes. Its bending stiffness was measured as 0.105N/mm by the typical three-point bending flexural test. Such a small bending stiffness value almost does not affect the bending motion of the continuum joint. The surgical instruments pass through the continuum joint's channel and open/close by the shell to passively unfold the instruments. Considering the size constraints, the maximum opening angle is designed to be 60° to ensure that the digestive tract wall will not be broken during operation and enhance surgical safety.

C. Optimization of the Proposed Continuum Joint

Optimizing structural parameters has been applied to improve the proposed continuum joint's bending and loading capabilities. In terms of bending capacity, the bending stiffness in the bending plane (K_b) of the continuum joint should be preferably low to reduce the tendon tension. Concerning loading capacity, the lateral stiffness induced by the external force applied perpendicularly to the bending plane (K_l) and torsional stiffness (K_t) should be sufficiently high to achieve a high loading capacity. Therefore, the objective function can be given as the maximum sum of stiffness ratios $\delta(X) = w_1 x_1 + w_2 x_2$, where w_1 and w_2 are weight coefficients, and the two stiffness ratios are defined as $x_1 = K_l/K_b$ and $x_2 = K_t/K_b$.

$$Y = \operatorname{Max} \delta(X) \tag{1}$$

$$\text{subject to} \begin{cases} w = \left[\frac{h_1+h_2}{2} - (2p - D)\tan\left(\frac{\alpha}{2}\right)\right]\cos\left(\frac{\alpha}{2}\right) > 1.5 \\ \alpha = 2\,\text{atan}\left(\frac{h_1}{2p}\right) < 8° \\ \theta_{\max} = \frac{2nh_1(2p-D)}{pD} > 100° \\ (n-1)(h_1 + h_2) + (1.5h_1 + 0.5h_1) = 80 \end{cases} \tag{2}$$

The constraint functions have also been defined in terms of design requirements and geometric relationships and listed as above. The minimum wall thickness needs to be larger than

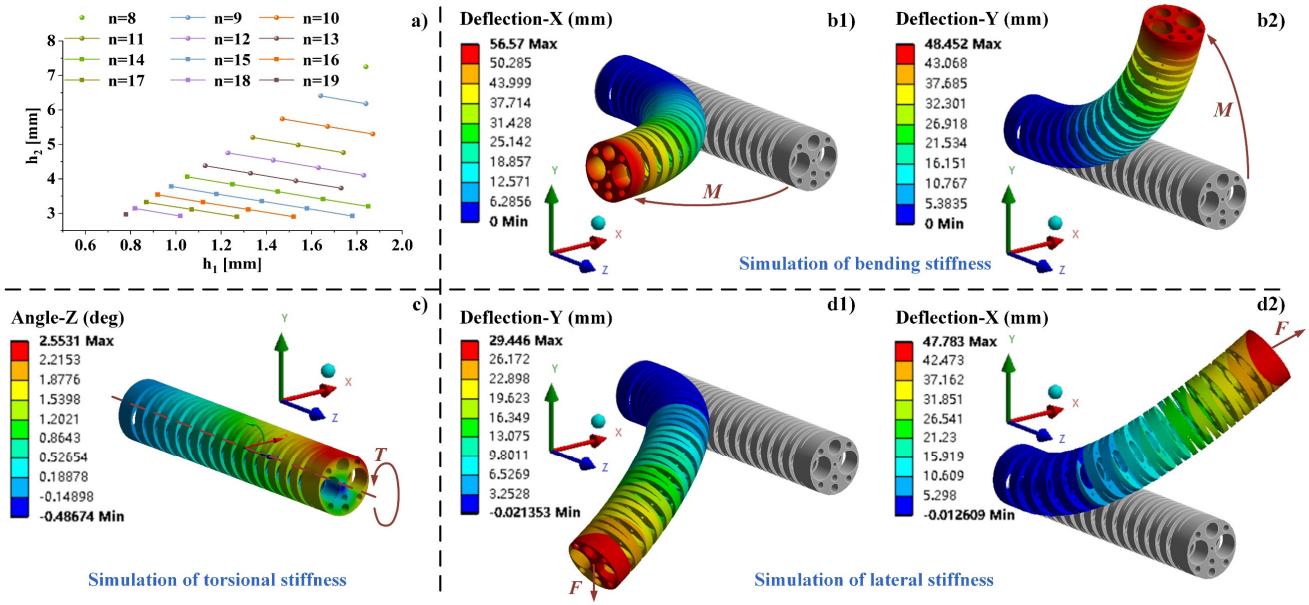

Fig. 3. a) The values of the structure parameters determined by the constraint functions; b) The moment is applied in the bending plane to investigate the bending stiffness; c) Torsional stiffness is simulated by applying torque to the distal end face; d) Radial force is applied perpendicularly to the bending plane to simulate the lateral stiffness.

1.5mm to avoid fracture under the limitation of the 3D printing processing. To avoid excessive deformation of Nylon materials, the design of the groove angle should not exceed 8°. The maximum bending angle should be larger than 100°, and the length of the distal continuum joint is 80mm. Since n is an integer, the value range of h_1 can be determined by Eq. (2) when n is of a different value and the value of h_1 is taken every 0.2mm within the value range according to the 3D printing precision. The values of w and h_2 can be calculated by constraint functions, and a total of 37 groups of solutions can be obtained, as shown in Fig. 3a). To optimize the design parameters, the finite element analysis (FEA) method is adopted to simulate the structure's rigidity due to the complexity of the mechanical structural model calculation. The entropy-weight analysis (EWA) method determines the weight coefficients.

In this work, FEA is performed by the static simulation provided by ANSYS Workbench 18.0. The continuum joint's fabrication material is Nylon PA12 (with Young's modulus of 1700MPa and Poisson's ratio of 0.4). Regarding the investigation of K_b, a force couple (±F and arm D/2) is utilized to replace a moment ($M = 100\text{mNm}$) [33]. The forces are applied to the distal end of the continuum joint, and the direction is invariably perpendicular to the end face as the continuum joint deflects, as shown in Fig. 3b). The torsional stiffness (K_t) can be obtained by applying torque ($T = 10\text{mNm}$) along the circumference of the continuum joint (Fig. 3c). To investigate K_l, a lateral force ($F = 0.5\text{N}$) is applied perpendicularly to the bending plane (Fig. 3d). At this point, x_1 and x_2 can be simulated and calculated by FEA. The entropy-weight analysis (EWA) method is utilized to determine the weight values of w_1 and w_2 according to the index variability. Firstly, the two indicators x_1 and x_2 are normalized. According to the above FEA simulation and calculation, there are 37 samples for each indicator. The normalized calculation is shown in Eq. (3).

$$\begin{cases} x_1' = \frac{x_1 - x_{1\min}}{x_{1\max} - x_{1\min}} \\ x_2' = \frac{x_2 - x_{2\min}}{x_{2\max} - x_{2\min}} \end{cases} \tag{3}$$

Secondly, the sample-specific gravity is calculated to obtain the information entropy and the entropy redundancy (Eq. (4)-Eq. (6)).

$$\begin{cases} p_1 = \frac{x_1'}{\sum x_1'} \\ p_2 = \frac{x_2'}{\sum x_2'} \end{cases} \tag{4}$$

$$\begin{cases} e_1 = -\frac{1}{\ln(i)} \sum p_1 \ln(p_1) \\ e_2 = -\frac{1}{\ln(i)} \sum p_2 \ln(p_2) \end{cases} \tag{5}$$

$$\begin{cases} d_1 = 1 - e_1 \\ d_2 = 1 - e_2 \end{cases} \tag{6}$$

where, p_1 and p_2 denotes the sample-specific gravity of x_1 and x_2; e_1 and e_2 represents the information entropy of x_1 and x_2 ; and d_1 and d_2 expresses the entropy redundancy of x_1 and x_2. i denotes the number of samples. Finally, the weight of each index can be calculated according to Eq. (7) as follows.

$$\begin{cases} w_1 = \frac{d_1}{d_1 + d_2} \\ w_2 = \frac{d_2}{d_1 + d_2} \end{cases} \tag{7}$$

Through the above calculation, w_1 and w_2 are determined as 0.405 and 0.595. The optimized parameters are summarized in Table II.

TABLE II
THE OPTIMIZED PARAMETERS OF THE CONTINUUM JOINT

Symbol	Value
h_1	1.52mm
h_2	2.90mm
p	14.5mm
w	1.53mm
α	6.44°
n	16

D. Workspace and Triangulation Analysis

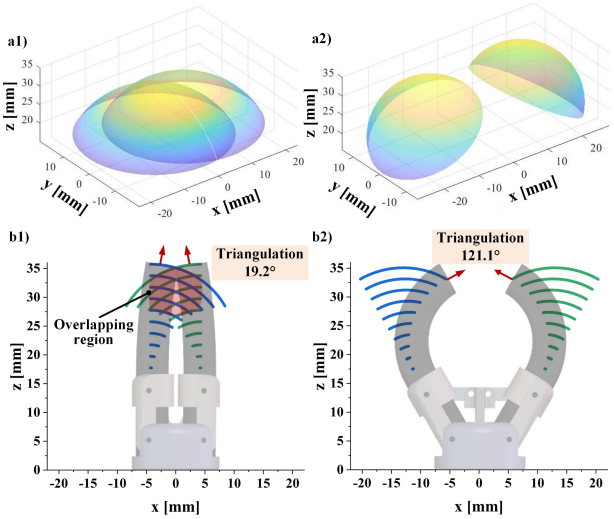

Fig. 4. Workspace and triangulation analysis: a) Workspace simulation without and with the deployable structure opening; b) Triangulation analysis without and with the deployable structure opening.

To evaluate the influence of the designed deployable structure on the workspace and triangulation of the two instruments, the simulation and analysis are performed via MATLAB 2019. Operational triangulation plays an essential role in dexterous examination and operations during flexible endoscopic surgery. The angle can be defined as the distal-end posture vectors between the two instruments [10]. The length of the bending section of each instrument is set at 20mm, and its maximum bending angle is 90°. The workspace and two-dimensional triangulation of the two instruments with and without the distal deployable structure opening have been illustrated in Fig. 4. The triangulation in the 2D plane has improved from 19.2° to 121.1° with the proposed deployable structure, increasing by 530.7%. This improvement is more conducive to cooperative operations. Besides, the spatial workspace of the two instruments overlaps significantly without the deployable structure opening. The overlapped region indicates two instruments' collision and motion interference to complete bimanual manipulations. This result

shows that the designed deployable structure can effectively avoid the collision of the two instruments during a cooperative task.

III. Experiments and Results

A. Experimental Setup

The experimental setup has been established to characterize the performances of the designed distal continuum joint, as illustrated in Fig. 5. It primarily consists of a prototyped 2-DOF notched continuum joint, a tendon-driving unit, four DC servomotors with gearboxes, a motion controller, four power amplifiers, and an optical tracking unit. The optimized continuum joint has been prototyped and connected with the driving unit. Four tendons in pairs are utilized to drive the continuum joint to achieve bending motion. Each DC motor (Maxon, DCX19S, Switzerland) equipped with a harmonic gearbox ratio of 103:1 (Maxon, GPX19, Switzerland) has been mounted on the tendon-driving unit to drive the tendons for tension and displacement transmission. The motion controller (OMRON, Power PMAC CK3M, Japan) generates the motion commands, which are subsequently amplified by the power amplifier (IMC, PNEP, Germany) to drive the DC servomotors. The optical tracking unit (Northern Digital Inc, Polaris Vega® ST, Canada) with a volumetric accuracy of 0.12mm has been employed to collect the actual trajectory of the distal tip. Three markers determine the base coordinate frame; another marker is fixed on the distal tip to measure the distal end position.

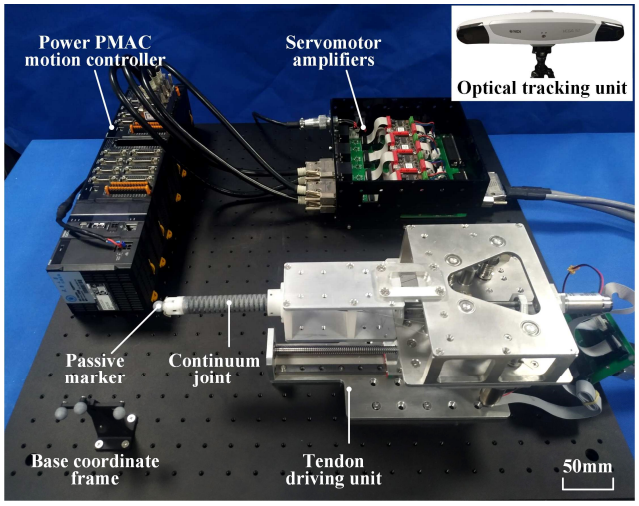

Fig. 5. Experimental setup for performance characterization of the designed continuum joint.

B. Characterization of the Constant Curvature Bending Performance

The designed continuum joint was bent within ±115° to evaluate its curvature characterization, as illustrated in Fig. 6a). Three repeated experiments were performed to collect the distal tip trajectory of the continuum joint in both two bending planes. These experimental values are compared with the theoretical values from constant curvature calculation [43], as detailed in Fig. 6b). Table III has calculated and listed average and maximum position error values. The distal tip position estimation yielded an average error of 1.36mm in the XZ plane and 1.10mm in the YZ plane based on the comparison between kinematics-derived results and the optical tracking sensor's results, accounting for 1.48% and 1.20% of the continuum joint's total length. The maximum relative position errors in the two bending planes were both less than 3.5%. These results indicate that the distal position values of the prototyped continuum joint are well consistent with the theoretical values, validating its excellent constant curvature characteristics.

The hysteresis errors were further investigated to evaluate the motion consistency during bending and releasing, as listed in Table III. The average error values were 0.81mm in the XZ plane and 0.58mm in the YZ plane, accounting for 0.89% and 0.64% of the total length. The maximum relative hysteresis errors of the continuum joint in the two bending planes were both less than 1.5%, demonstrating its inappreciable hysteresis error and outstanding motion consistency in the bending and releasing phases. Please be aware that the designed continuum joint exhibits slightly different bending characteristics in the two planes. However, the difference is still minor (less than 1.2%, ranging from 0.26mm to 1.07mm calculated by Table III). This difference is mainly caused by fabrication and assembly errors. Especially, it is challenging to regulate the pre-tension of the four driving tendons as the same value. The differences in pre-tension can lead to a slightly varying performance in both bending planes. In other researchers' investigations, more distinct bending performances in two bending planes have been observed [44-46]. The integration of proximal force sensors onto the driving unit will be investigated to measure and adjust the tendons' pre-tension forces to lower such differences between different bending planes [47].

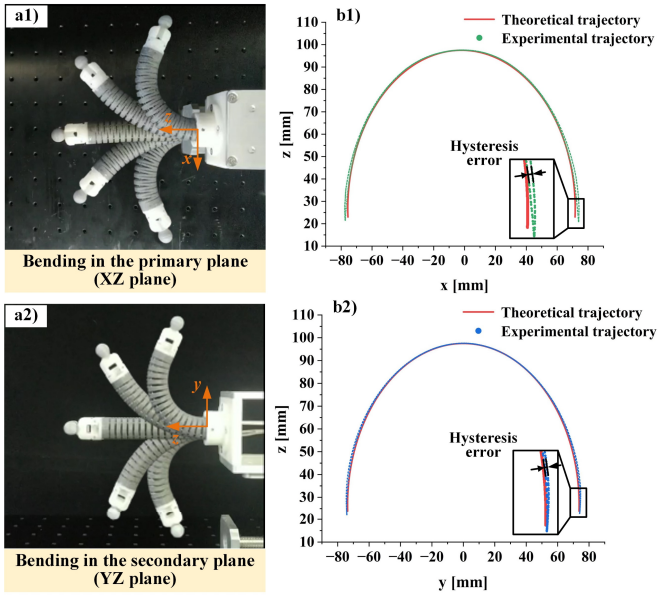

Fig. 6. Curvature characterization of the proposed continuum joint in two planes: a1) Bending in the primary plane (XZ plane); a2) Bending in the secondary plane (YZ plane); b1) The experimental and theoretical trajectory in the XZ plane; b2) The experimental and theoretical trajectory in the YZ plane.

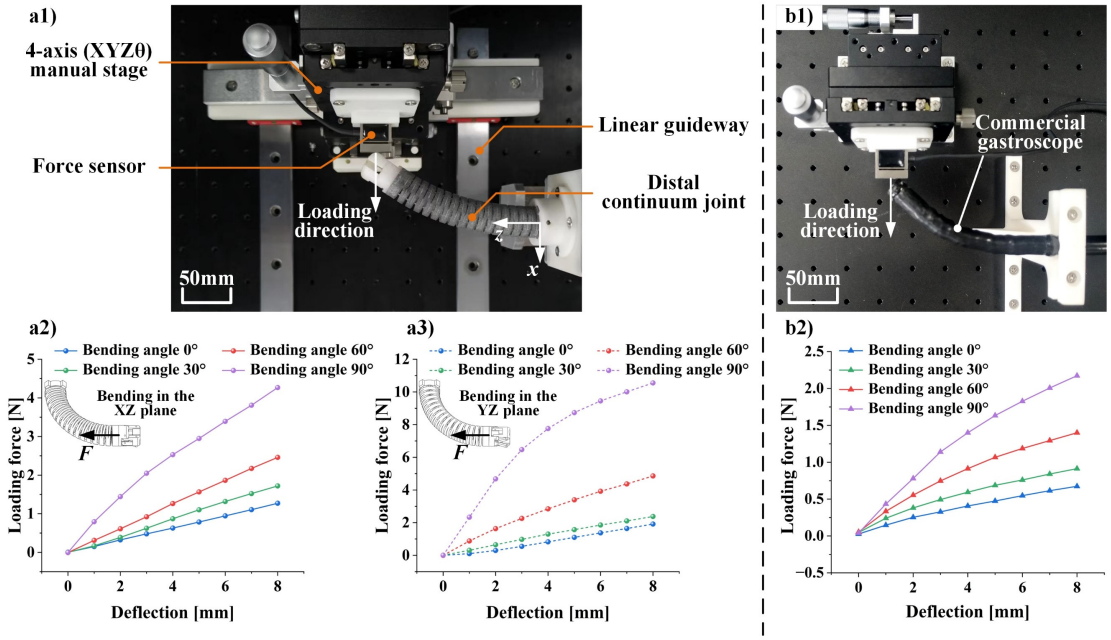

Fig. 7. Quantification for the loading capacity when the forces applied along the bending planes: a1) Experimental setup of the designed continuum joint; a2) Experimental results of bending in the XZ plane; a3) Experimental results of bending in the YZ plane; b1) Experimental setup of the commercial gastroscope; b2) Experimental results of the commercial gastroscope.

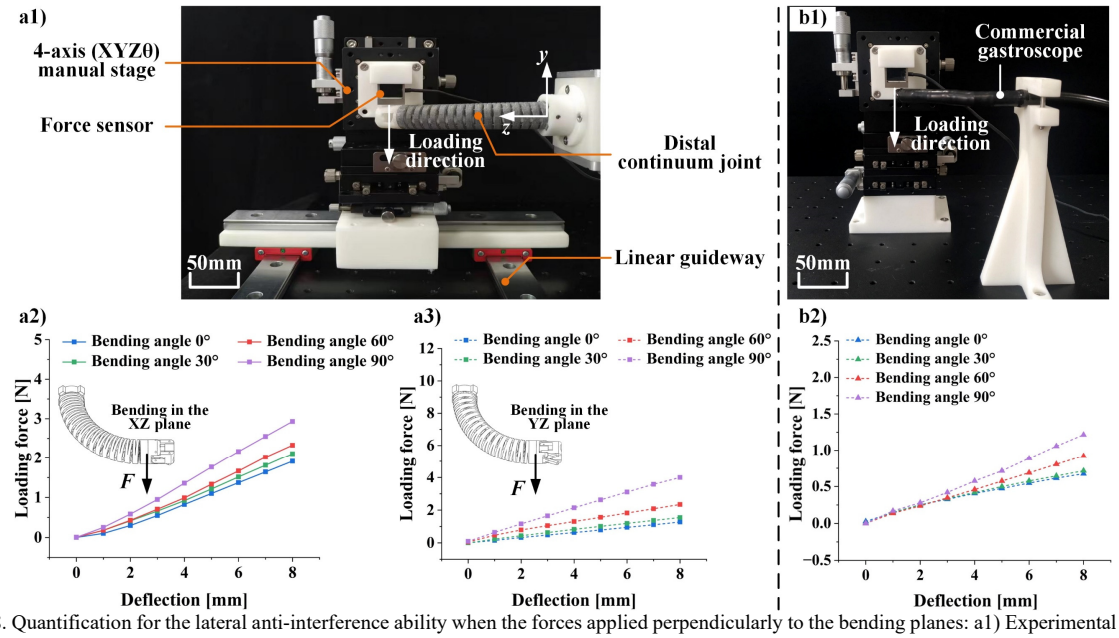

Fig. 8. Quantification for the lateral anti-interference ability when the forces applied perpendicularly to the bending planes: a1) Experimental setup of the designed continuum joint; a2) Experimental results of bending in the XZ plane; a3) Experimental results of bending in the YZ plane; b1) Experimental setup of the commercial gastroscope; b2) Experimental results of the commercial gastroscope.

TABLE III
THE POSITIONING AND HYSTERESIS ERROR VALUES OF THE PROPOSED CONTINUUM JOINT

	Average position error (*)	Maximum position error (*)	Average hysteresis error (*)	Maximum hysteresis error (*)
XZ plane	1.36mm (1.48%)	3.11mm (3.40%)	0.81mm (0.89%)	1.36mm (1.48%)
YZ plane	1.10mm (1.20%)	2.04mm (2.23%)	0.58mm (0.64%)	1.05mm (1.15%)

* Relative error accounting for the total length of the continuum joint.

C. Quantification for the Loading Capacity

The distal loading experiments have been performed to investigate the loading capacity when the forces are applied along the bending plane, as illustrated in Fig. 7. For a flexible endoscopic robot, the distal deflection of less than 10% of the continuum joint's total length can be corrected by the surgeon under visual guidance [48]. Therefore, the loading test was performed within 8mm of the distal deflection to evaluate the loading capacity. A force sensor (JinNuo, JLBS-M2, China) with a resolution of 10mN was mounted on a 4-axis (XYZθ)

stage and moved by the manual stage with an internal step of 1mm to measure the distal force, as shown in Fig. 7 a1). The same procedure was then repeated three times with the bending angles of 0°, 30°, 60°, and 90° respectively. The corresponding loading values are shown in Fig. 7 a2-a3). To further compare with the commercial gastroscope, the loading capacity was tested in a similar manner, as shown in Fig. 7 b1). The commercial gastroscope (AOHUA, VME98, China) with an outer diameter of 9.2mm was fixed on the 3-D printed support. The corresponding results were plotted in Fig. 7 b2). In addition, the lateral anti-interference ability has also been investigated by applying the force perpendicularly to the bending plane, as shown in Fig. 8. The experimental process was similar to the above-mentioned case, and the results have been plotted in Fig. 8 a2)-a3) and Fig. 8 b2).

As summarized in Table IV, when the joint's bending angle reached 90°, the loading capability of the proposed continuum design achieved the maximum value. For the case of the force applied along the bending plane, the loading force was 4.27N in the XZ plane and 10.55N in the YZ plane, respectively, corresponding to 1.97 times and 4.86 times of the commercial gastroscope. For the case of the force applied perpendicularly to the bending plane, the values of resistance forces were 2.93N (in the XZ plane) and 4.00N (in the YZ plane), corresponding to 2.42 times and 3.31 times of the commercial gastroscope. Even when the continuum joint was in the initial state (the bending angle was 0°), it could still withstand a certain amount of the external loading of 1.27N and 1.91N, which is 1.9 times and 2.85 times that for the commercial endoscope. These results reveal that the designed continuum joint provides significant advantages in terms of a higher loading capacity over the commercial endoscope. It is worth noting that the loading capacity reached 10.55N when bending in the YZ plane. This occurs because of the geometric error of the notches induced by insufficient 3D printing accuracy. The notches are in contact with each other at a large bending angle, and the internal force increases significantly, resulting in greater loading capacity than other data groups.

TABLE IV
THE EXPERIMENTAL VALUES OF LOADING CAPACITY TESTS OF THE PROPOSED CONTINUUM JOINT AND THE COMMERCIAL GASTROSCOPE

	Bending angle [deg]	Loading force [N]	
		Along to the bending plane	Perpendicular to the bending plane
The proposed continuum joint (Bending in the XZ plane)	0	1.27	1.91
	30	1.72	2.11
	60	2.46	2.33
	90	4.27	2.93
The proposed continuum joint (Bending in the YZ plane)	0	1.91	1.27
	30	2.38	1.55
	60	4.86	2.34
	90	10.55	4.00
The commercial gastroscope	0	0.67	0.67
	30	0.91	0.71
	60	1.40	0.92
	90	2.17	1.21

D. Investigation for the Torsional Stiffness

The experimental setup to quantify the twisting capacity of the continuum joint has been illustrated in Fig. 9a). The distal end of the designed continuum joint was connected with a torque sensor (HIOS, HP-10, Japan) for twisting torque collection, and the proximal end was configured with a DC servomotor by a coupler. The DC motor drove the prototyped continuum joint to produce a torsion angle with an interval step of 2°. The linear least square fitting method was used to fit the experimental data to determine the torque-torsion angle relationship, as shown in Fig. 9b). The experimental torsional stiffness value of the proposed continuum joint was calculated to achieve 8.73mNm/°. This result was more than twice that of other research [35, 36]. It proves that the designed continuum joint can withstand relatively large torque inputs, which benefits providing stable support for instruments during surgical operations.

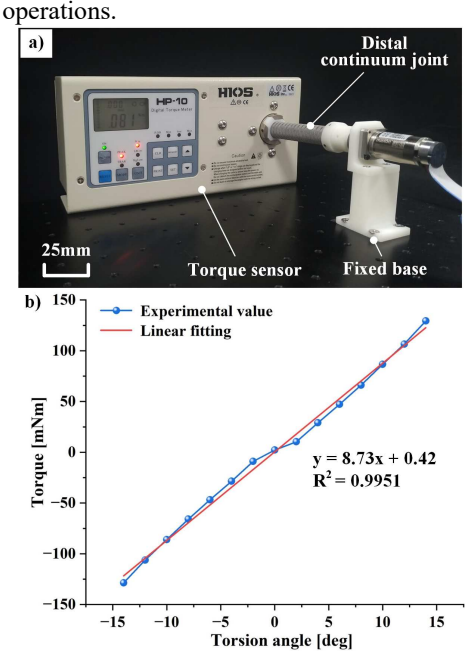

Fig. 9. a) Experimental setup for the torsional stiffness test; b) The experimental results.

E. Ex-vivo tests

An ex-vivo experimental test for gastric tissue biopsy was carried out to investigate the effectiveness of the proposed continuum overtube in a practical scenario. The detailed experimental setup includes the tendon driving unit with servomotor amplifiers, a motion controller, the designed continuum overtube mounted at the distal end of a 350mm length of soft rubber tube, a porcine stomach (about 500g) with a simulated esophagus (made by a transparent PVC tube), as displayed in Fig. 10a). Two customized instruments was retrofitted by commercial bronchoscope (Shiqing Trade Center, CN, OD = 5mm) to perform the bimanual operation. Two male participants (with an average age of 25) from Tianjin University were recruited as research staff for the ex-vivo experiments. They have no relevant medical background or experience in performing surgical procedures. After obtaining their informed consent, these participants received training on the bimanual

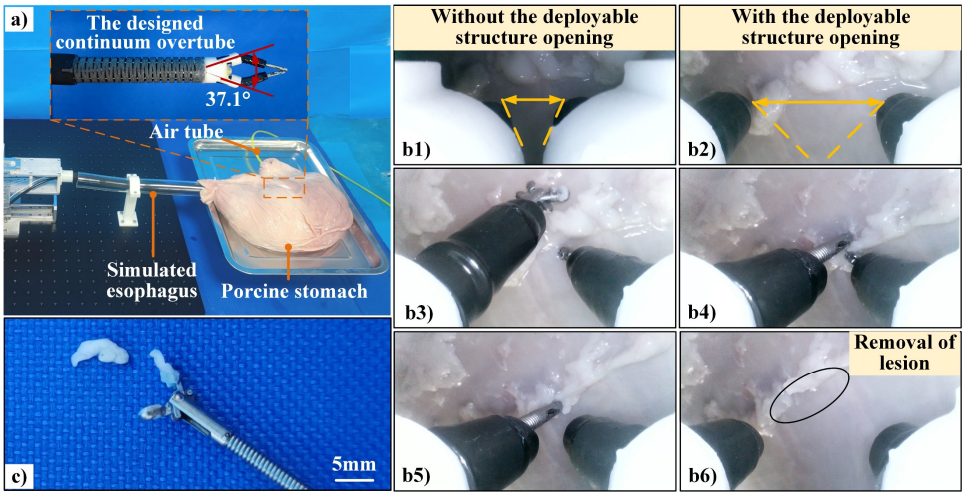

Fig. 10. a) Ex-vivo experimental setup; b) The operation process: b1) Approach at the lesion; b2) Triangulation formed by the deployable structure opening; b3)-b5) Resection of the lesion with two instruments; b6) Removal of lesion; c) Display of the diseased tissue.

operation of instruments and then maneuvered the designed continuum overtube. The training process was followed by approximately 20 minutes of individual practice. When the deployable structure was opened, the two instruments formed an improved triangulation, as shown at the top of Fig. 10a). The pneumoperitoneum was created by passing the air produced by the air compressor (1600W-30L, OTS, CN) into the porcine stomach through the tube (labeled in yellow in Fig. 10a).

During the operation, the tendon driving unit drove the continuum overtube to guide along the simulated esophagus and advance inside the porcine stomach, as shown in Fig. 10 b1). After accessing the lesion, the distal deployable structure was opened by driving the flexible shaft to support the two instruments to form a more extensive triangulation, as shown in Fig. 10 b2). The two surgical instruments were maneuvered to approach the operation area and then grasped and pulled the target tissue, as illustrated in Fig. 10 b3) - b5). Finally, the biopsy and sampling of the diseased tissue are completed by instrument cooperation, as displayed in Fig. 10 b6) and Fig. 10c). After simple training, the operation duration of endoscopic bimanual biopsy was typically about 3 minutes. The deployable structure was conducive to improving the operational triangulation, avoiding the interference of instruments collision, and enlarging the surgical field of vision. This experiment validates the feasibility of utilizing the continuum overtube in flexible endoscopic surgery. Besides, the proposed design can potentially carry out EMR or ESD procedures by replacing the biopsy forceps with a snare or hook knife.

IV. Discussion

An overview of the performance comparison with other types of continuum joints can be found in Table V. The proposed triangular notched continuum joint benefiting from the deeply-cutting design, enables 2-DOF deflection (bending in the 3D space) with only one segment, thereby improving the motion flexibility and reachable workspace. Moreover, the proposed design utilizes specialized triangular notches and increases the overlapping area between the notches to generate evenly distributed stress, leading to excellent constant curvature bending characteristics in an extensive motion range of ±115°. Besides, the relative maximum position error values are 3.40% and 2.23% in the two bending planes. It can effectively predict the distal trajectory of the constructed continuum joint with better distal positioning accuracy based on the assumption of constant bending curvature. In addition, the maximum relative hysteresis errors in the two bending planes are both less than 1.5%, indicating excellent motion consistency during bending and releasing.

The continuum-style joints commonly generate large tension forces of driving tendons due to the deflection induced by the material's deformation and achieve improved loading capacity, as indicated in Table V. For instance, Lee et al. [28] proposed a 2-DOF continuum overtube utilizing the rectangular slit structure with rigid supporters for flexible endoscopy, which can resist an external loading of 7N. However, the complex structure resulted in a larger diameter of 23mm and faced difficulties applying it in a practical scenario. In this work, the structural parameters optimization approach has been implemented to balance the trade-off between the continuum joint's bending and loading capabilities by adjusting the notches parameters. Thus, excellent bending performances can be preserved, and meanwhile, the loading capacity of the designed continuum joint can achieve larger than 4.27N (in the case of the loading force applied within the bending plane), which is sufficient for most endoscopic operations. Furtherly, the lateral resistance force is greater than 2.93N (in the case of the loading force applied out of the bending plane), which is rarely mentioned in other works, proving that the designed continuum has a solid lateral anti-interference ability.

Moreover, anti-torsion capability also poses a challenge for the design of continuum joints, particularly for lengthy structures. The slender continuum joint designs with a high length-to-diameter ratio are more suitable for operation in confined spaces. However, they commonly suffer from twisting along their axial direction due to the torque induced by the distal

TABLE V
THE PERFORMANCE COMPARISON OF SEVERAL CONTINUUM JOINTS

Group	Style	Bending range	DOF	Relative maximum position error	Relative maximum hysteresis error	Loading capacity(1)	Lateral anti-interference ability(2)	Torsional stiffness	OD	Functional channels and triangulation(5)
Kim et al [18]	Discrete	±180°	1	4.25%	7.87%	2.5N	\	\	15.9mm	1/ WO
Sefati et al [42]	Continuum	±90°	1	5.14%	\	< 1N	< 1.3N	\	5.99mm	1/ WO
Lee et al [28]	Continuum	±90°	2	\	\	7N	\	\	23mm	4/ WO
Zhang et al [36]	Continuum	±60°	2	12.9%	4.65%	\	\	≈1.67mNm/° (simulated)	10mm	1/ WO
Song et al [35]	Continuum	±180°	1	5.01%	0.95%	5N	\	4.06mNm/°	12mm	1/ WO
This work	**Continuum**	**±115°**	**2**	**3.40%(3) 2.23%(4)**	**1.48%(3) 1.15%(4)**	**4.27N(3) 10.55N(4)**	**2.93N(3) 4.00N(4)**	**8.73mNm/°**	**16mm**	**3/ W**

(1) Force is applied along the bending plane; (2) Force is applied perpendicularly to the bending plane; (3) Bending in the XZ plane; (4) Bending in the YZ plane; (5) WO: without triangulation, W: with triangulation.

payload. Insufficient anti-torsion capacity can result in noticeable rotation inconsistency between the proximal and distal parts of the joints, as well as inadequate loading capacity under external payloads, thereby degrading the control accuracy [49]. To address this difficulty, both the central arrangement of the Nitinol backbone and the optimization of the notched continuum joint's structural parameters have been employed to enhance the anti-torsion capacity of the continuum joint. However, the proposed optimization approach primarily focuses on optimizing the triangular notched structure and intends to achieve a trade-off between the bending and loading capabilities. It can improve the torsion resistance of the continuum joint to some extent but with limited effects. Therefore, the Nitinol central backbone is specially arranged to further improve the anti-torsion and anti-compression capabilities of the continuum joint during bending. The torsional stiffness of the proposed continuum joint achieves 8.73mNm/°, much greater than the type of spring structure-based continuum joint, as listed in Table V.

Furthermore, the number and size of functional channels within the existing continuum joints have also been compared. The presented design has an outer diameter of 16mm and provides outstanding integration performance for bimanual operation. Although four channels for the endoscope and instruments had been reserved inside the continuum joint [28], there was a lack of consideration for triangulation. In this work, the distal deployable structure has been integrated with the continuum joint and is conducive to improving the operational triangulation for bimanual operation and some complex diagnostic or therapeutic procedures. Besides, commercial endoscopes utilized to examine the digestive tracts typically have an outer diameter of 9-15mm. They are typically equipped with a CCD module and an objective lens for providing visual information, a water jet for rinsing the lens, an air/water nozzle for clearing the internal effusion, and one instrument channel for operation. If two instruments are required to be carried by the flexible endoscope, the diameter will undoubtedly increase. Therefore, the designed outer diameter is appropriate for gastrointestinal applications within a range of 16 to 22mm. This design can be further reduced in outer diameter by using metal 3D printing technology with higher precision or by replacing the instrument arm with a slenderer one.

V. CONCLUSION

A novel continuum overtube consisting of a tendon-driven notched 2-DOF continuum joint and a distal deployable triangulation. The presented overtube offers advantages in terms of high flexibility, outstanding properties of constant bending curvature, sufficient loading and anti-twisting capacity and convenient integration with surgical instruments, and extensive operational triangulation. Moreover, the employed design optimization provides a guideline for performance improvement of the continuum joint. The deployable structure's introduction can effectively improve the triangulation for cooperative operations and support bimanual manipulations to address complex tissue interventions in the ESD procedures. Characterization experiments have been conducted to evaluate the performances of the overtube in terms of bending characteristics, loading capacity, and anti-twisting properties. Ex-vivo tests have been performed to demonstrate its feasibility in flexible endoscopy. Future work will further consider the robotization and integration of the instruments and FBG-based shape and distal force sensors [50-52] with the proposed overtube to form a flexible endoscopic robotic system.

REFERENCES

[1] V. Vitiello, S. L. Lee, T. P. Cundy *et al.*, "Emerging robotic platforms for minimally invasive surgery," *IEEE Rev Biomed Eng,* vol. 6, no. 1, pp. 111-126, Mar, 2013.
[2] P. E. Dupont, B. J. Nelson, M. Goldfarb *et al.*, "A decade retrospective of medical robotics research from 2010 to 2020," *Sci Robot,* vol. 6, no. 60, pp. eabi8017, Nov, 2021.
[3] C. Shi, X. Luo, P. Qi *et al.*, "Shape sensing techniques for continuum robots in minimally invasive surgery: A survey," *IEEE Trans Biomed Eng,* vol. 64, no. 8, pp. 1665-1678, Aug, 2017.
[4] M. T. Thai, P. T. Phan, T. T. Hoang *et al.*, "Advanced intelligent systems for surgical robotics," *Adv Intell Syst,* vol. 2, no. 8, pp. 1900138, Jun, 2020.
[5] P. W. Chiu, "Novel endoscopic therapeutics for early gastric cancer," *Clin Gastroenterol Hepatol,* vol. 12, no. 1, pp. 120-5, Jan, 2014.

[6] J. Kim, M. de Mathelin, K. Ikuta *et al.*, "Advancement of flexible robot technologies for endoluminal surgeries," *Proc. IEEE,* vol. 110, no. 7, pp. 909-931, Jul, 2022.
[7] J. Zhu, L. Lyu, Y. Xu *et al.*, "Intelligent soft surgical robots for next-generation minimally invasive surgery," *Adv Intell Syst,* vol. 3, no. 5, pp. 2100011, May, 2021.
[8] J. Burgner-Kahrs, D. C. Rucker, and H. Choset, "Continuum robots for medical applications: A survey," *IEEE Trans Robot,* vol. 31, no. 6, pp. 1261-1280, Dec, 2015.
[9] Y. Zhong, L. Hu, and Y. Xu, "Recent advances in design and actuation of continuum robots for medical applications," *Actuators,* vol. 9, no. 4, pp. 142, Dec, 2020.
[10] E. A. Arkenbout, P. W. Henselmans, F. Jelinek *et al.*, "A state of the art review and categorization of multi-branched instruments for NOTES and SILS," *Surg Endosc,* vol. 29, no. 6, pp. 1281-96, Jun, 2015.
[11] N. Simaan, R. M. Yasin, and L. Wang, "Medical technologies and challenges of robot-assisted minimally invasive intervention and diagnostics," *Annu Rev Control Robot Auton Syst,* vol. 1, no. 1, pp. 465-490, May, 2018.
[12] T. da Veiga, J. H. Chandler, P. Lloyd *et al.*, "Challenges of continuum robots in clinical context: A review," *Prog. Biomed. Eng.,* vol. 2, no. 3, pp. 032003, Jul, 2020.
[13] P. E. Dupont, N. Simaan, H. Choset *et al.*, "Continuum robots for medical interventions," *Proc. IEEE,* vol. 110, no. 7, pp. 847-870, Jul, 2022.
[14] F. Jelínek, E. A. Arkenbout, P. W. J. Henselmans *et al.*, "Classification of joints used in steerable instruments for minimally invasive surgery: A review of the state of the art," *J Med Device,* vol. 9, no. 1, pp. 010801, Mar, 2015.
[15] C. Li, Y. Yan, X. Xiao *et al.*, "A miniature manipulator with variable stiffness towards minimally invasive transluminal endoscopic surgery," *IEEE Robot Autom Lett,* vol. 6, no. 3, pp. 5541-5548, Jul, 2021.
[16] W. Hong, L. Xie, J. Liu *et al.*, "Development of a novel continuum robotic system for maxillary sinus surgery," *IEEE-ASME Trans Mechatron,* vol. 23, no. 3, pp. 1226-1237, Jun, 2018.
[17] M. Hwang, and D.-S. Kwon, "Strong continuum manipulator for flexible endoscopic surgery," *IEEE-ASME Trans Mechatron,* vol. 24, no. 5, pp. 2193-2203, Oct, 2019.
[18] H. Kim, J. M. You, M. Hwang *et al.*, "Sigmoidal auxiliary tendon-driven mechanism reinforcing structural stiffness of hyper-redundant manipulator for endoscopic surgery," *Soft Robot*, Jun, 2022.
[19] X. Zhang, W. Li, P. W. Y. Chiu *et al.*, "A novel flexible robotic endoscope with constrained tendon-driven continuum mechanism," *IEEE Robot Autom Lett,* vol. 5, no. 2, pp. 1366-1372, Apr, 2020.
[20] W. Hong, F. Feng, L. Xie *et al.*, "A two-segment continuum robot with piecewise stiffness for maxillary sinus surgery and its decoupling method," *IEEE-ASME Trans Mechatron,* vol. 27, no. 6, pp. 4440-4450, Dec, 2022.
[21] J. W. Suh, K. Y. Kim, J. W. Jeong *et al.*, "Design considerations for a hyper-redundant pulleyless rolling joint with elastic fixtures," *IEEE-ASME Trans Mechatron,* vol. 20, no. 6, pp. 2841-2852, Dec, 2015.
[22] G. Arora, A. Mannalithara, G. Singh *et al.*, "Risk of perforation from a colonoscopy in adults: A large population-based study," *Gastrointest Endosc,* vol. 69, no. 3 Pt 2, pp. 654-64, Mar, 2009.
[23] G. Ciuti, K. Skonieczna-Zydecka, W. Marlicz *et al.*, "Frontiers of robotic colonoscopy: A comprehensive review of robotic colonoscopes and technologies," *J Clin Med,* vol. 9, no. 6, pp. 1648, May, 2020.
[24] W. Marlicz, X. Ren, A. Robertson *et al.*, "Frontiers of robotic gastroscopy: A comprehensive review of robotic gastroscopes and technologies," *Cancers (Basel),* vol. 12, no. 10, pp. 2775, Sep, 2020.
[25] J. Gafford, M. Freeman, L. Fichera *et al.*, "Eyes in ears: A miniature steerable digital endoscope for trans-nasal diagnosis of middle ear disease," *Ann Biomed Eng,* vol. 49, no. 1, pp. 219-232, Jan, 2021.
[26] Y. Chitalia, S. Jeong, N. Deaton *et al.*, "Design and kinematics analysis of a robotic pediatric neuroendoscope tool body," *IEEE-ASME Trans Mechatron,* vol. 25, no. 2, pp. 985-995, Apr, 2020.
[27] Y. Chitalia, S. Jeong, K. K. Yamamoto *et al.*, "Modeling and control of a 2-DoF meso-scale continuum robotic tool for pediatric neurosurgery," *IEEE Trans Robot,* vol. 37, no. 2, pp. 520-531, Apr, 2021.
[28] J. H. Lee, W. H. Shin, and D. S. Kwon, "A modularized wire-driven overtube using tube type bending mechanism for robotic NOTES system," *2013 13th International Conference on Control, Automation and Systems (ICCAS)*, pp. 631-634, 2013.
[29] H. D. Wang, X. L. Wang, W. L. Yang *et al.*, "Design and kinematic modeling of a notch continuum manipulator for laryngeal surgery," *International Journal of Control Automation and Systems,* vol. 18, no. 11, pp. 2966-2973, Nov, 2020.
[30] E. Amanov., Josephine Granna, and J. Burgner-Kahrs, "Toward improving path following motion: Hybrid continuum robot design," in *IEEE International Conference on Robotics and Automation (ICRA)*, Singapore, 2017, pp. 4666-4672.
[31] Z. Wang, S. Bao, B. Zi *et al.*, "Development of a novel 4-DOF flexible endoscopic robot using cable-driven multisegment continuum mechanisms," *J Mech Robot,* vol. 16, no. 3, pp. 031011, Mar, 2024.
[32] Z. J. Du, W. L. Yang, and W. Dong, "Kinematics modeling of a notched continuum manipulator," *J Mech Robot,* vol. 7, no. 4, pp. 041017, Nov, 2015.
[33] Y. Hu, L. Zhang, W. Li *et al.*, "Design and fabrication of a 3-D printed metallic flexible joint for snake-like surgical robot," *IEEE Robot Autom Lett,* vol. 4, no. 2, pp. 1557-1563, Apr, 2019.
[34] W. Li, M. Shen, A. Gao *et al.*, "Towards a snake-like flexible robot for endoscopic submucosal dissection," *IEEE Trans Med Robot Bionics,* vol. 3, no. 1, pp. 257-260, Feb, 2021.
[35] Y. Song, S. Wang, X. Luo *et al.*, "Design and optimization of a 3D printed distal flexible joint for endoscopic surgery," *IEEE Trans Med Robot Bionics,* vol. 4, no. 1, pp. 38-49, Feb, 2022.
[36] X. Zhang, Y. T. Xian, Z. W. Cui *et al.*, "Design and modeling of a novel DNA-inspired helix-based continuum mechanism (DHCM)," *Mech Mach Theory,* vol. 171, no. 1, pp. 104702, May, 2022.
[37] X. Luo, D. Song, Z. Zhang *et al.*, "A novel distal hybrid pneumatic/cable-driven continuum joint with variable stiffness capacity for flexible gastrointestinal endoscopy," *Adv Intell Syst*, pp. 2200403 2023.
[38] V. D. Sars, S. Haliyo, and J. Szewczyk, "A practical approach to the design and control of active endoscopes," *Mechatronics,* vol. 20, no. 2, pp. 251-264, Mar, 2010.
[39] M. Hwang, and D. S. Kwon, "K-FLEX: A flexible robotic platform for scar-free endoscopic surgery," *Int J Med Robot,* vol. 16, no. 2, pp. e2078, Apr, 2020.
[40] K. C. Lau, E. Y. Y. Leung, P. W. Y. Chiu *et al.*, "A Flexible Surgical Robotic System for Removal of Early-Stage Gastrointestinal Cancers by Endoscopic Submucosal Dissection," *IEEE Trans Industr Inform,* vol. 12, no. 6, pp. 2365-2374, Dec, 2016.
[41] F. Alambeigi, M. Bakhtiarinejad, S. Sefati *et al.*, "On the use of a continuum manipulator and a bendable medical screw for minimally invasive interventions in orthopedic surgery," *IEEE Trans Med Robot Bionics,* vol. 1, no. 1, pp. 14-21, Feb, 2019.
[42] S. Sefati, R. Hegeman, I. Iordachita *et al.*, "A dexterous robotic system for autonomous debridement of osteolytic bone lesions in confined spaces: Human cadaver studies," *IEEE Trans Robot,* vol. 38, no. 2, pp. 1213-1229, Apr, 2022.
[43] R. J. Webster, and B. A. Jones, "Design and kinematic modeling of constant curvature continuum robots: A review," *Int J Rob Res,* vol. 29, no. 13, pp. 1661-1683, Nov, 2010.
[44] D. Wu, J. Li, D. Song *et al.*, "Development of a novel ball-and-socket flexible manipulator for minimally invasive flexible surgery," *IEEE Trans Med Robot Bionics,* vol. 5, no. 2, pp. 278-288, May, 2023.
[45] X. Wang, J. Yan, X. Ma *et al.*, "Hybrid-structure hand-held robotic endoscope for sinus surgery with enhanced distal dexterity," *IEEE-ASME Trans Mechatron,* vol. 27, no. 4, pp. 1863-1872, Aug, 2022.
[46] J. Yan, J. Chen, J. Chen *et al.*, "A continuum robotic cannula with tip following capability and distal dexterity for intracerebral hemorrhage evacuation," *IEEE Trans Biomed Eng,* vol. 69, no. 9, pp. 2958-2969, Sep, 2022.
[47] J. Hao, D. Song, C. Hu *et al.*, "Two-dimensional shape and distal force estimation for the continuum robot based on learning from the proximal sensors," *IEEE Sens J,* vol. 23, no. 10, pp. 10836-10846, May, 2023.
[48] X. Gu, C. Li, X. Xiao *et al.*, "A compliant transoral surgical robotic system based on a parallel flexible mechanism," *Ann Biomed Eng,* vol. 47, no. 6, pp. 1329-1344, Jun, 2019.
[49] X. Dong, M. Raffles, S. Cobos-Guzman *et al.*, "A novel continuum robot using twin-pivot compliant joints: Design, modeling, and validation," *J Mech Robot,* vol. 8, no. 2, pp. 021010, May, 2016.
[50] C. Shi, X. Luo, J. Guo *et al.*, "Three-dimensional intravascular reconstruction techniques based on intravascular ultrasound: A technical review," *IEEE J Biomed Health Inform,* vol. 22, no. 3, pp. 806-817, May, 2018.
[51] K. Sun, M. Li, S. Wang *et al.*, "Development of a fiber bragg grating-enabled clamping force sensor integrated on a grasper for laparoscopic surgery," *IEEE Sens J,* vol. 21, no. 15, pp. 16681-16690, Aug, 2021.